applied sciences

MDPI

*Article*

# Dosimetric Effect of Injection Ports in Tissue Expanders on Post-Mastectomy Volumetric Modulated Arc Therapy (VMAT) Planning for Left-Sided Breast Cancer

**Na-Hyun Hwang [1], Myungsoo Kim [2,*], Nam Kwon Lee [3], Suk Lee [3] and Jinho Hwang [2]**

[1] Department of Plastic and Reconstructive Surgery, Korea University Anam Hospital, Korea University College of Medicine, Seoul 02841, Korea; prissy426@gmail.com
[2] Department of Radiation Oncology, Incheon St. Mary's Hospital, College of Medicine, The Catholic University of Korea, Seoul 06591, Korea; b75365817@gmail.com
[3] Department of Radiation Oncology, Korea University Anam Hospital, Korea University College of Medicine, Seoul 02841, Korea; nklee74@korea.ac.kr (N.K.L.); sukmp@korea.ac.kr (S.L.)
* Correspondence: mskim0710@gmail.com

**Abstract:** This study aimed to compare the dosimetric effect of traditional metallic ports and radio frequency identification (RFID) ports (Motiva Flora®) on post-mastectomy volumetric modulated arc therapy (VMAT) planning for left-sided breast cancer. Computed tomography (CT) simulation was performed on an anthropomorphic torso phantom by attaching two types of tissue expander on the left chest wall. For the comparison of CT artifacts, five points of interest were selected and compared: point A = central chest wall, B = medial chest wall, point C = lateral chest wall, point D = axilla, and point E = left anterior descending artery. VMAT planning using two partial arcs with a single isocenter was generated, and dosimetric parameters were investigated. Compared to metallic ports, RFID ports tremendously decreased distortion on CT images, with the exception of point D. The $V_{5Gy}$, $V_{10Gy}$, $V_{15Gy}$, $V_{20Gy}$, $V_{30Gy}$, and $D_{mean}$ values of the heart in RFID ports were lower than those in metallic ports. The $V_{5Gy}$, $V_{15Gy}$, $V_{20Gy}$, $V_{30Gy}$, and $D_{mean}$ values of the ipsilateral lung in RFID ports were also lower than those in metallic ports. RFID ports showed superior dosimetric results for doses to the heart and lungs as compared to that in metallic ports.

**Keywords:** tissue expander; breast cancer; radiotherapy; volumetric modulated arc therapy



**Citation:** Hwang, N.-H.; Kim, M.; Lee, N.K.; Lee, S.; Hwang, J. Dosimetric Effect of Injection Ports in Tissue Expanders on Post-Mastectomy Volumetric Modulated Arc Therapy (VMAT) Planning for Left-Sided Breast Cancer. *Appl. Sci.* **2022**, *12*, 6461. https://doi.org/10.3390/app12136461

Academic Editor: Qi-Huang Zheng

Received: 2 June 2022
Accepted: 22 June 2022
Published: 25 June 2022



## 1. Introduction

Breast reconstruction is a cosmetic option for patients receiving mastectomy. Since the introduction of breast implants as an option for immediate breast reconstruction following mastectomy in the 1960s, the use of prostheses has exceeded that of autologous tissue reconstruction in the early 2000s [1]. The most commonly practiced form of implant-based breast reconstruction to date is the two-stage rather than single-stage direct-to-implant reconstruction [2]. The two-stage prosthetic breast reconstruction process involves insertion of a tissue expander into the pocket created after mastectomy. The expander undergoes saline inflation to stretch the dimensions of the retained skin envelope and to avoid wound contraction during wound maturation. Once the skin is sufficiently stretched, the expanders are removed and replaced with breast implants. Moreover, the development of tissue expanders by Radovan has created new possibilities in immediate and delayed reconstructions [3,4]. Currently, more than 70% of all breast reconstruction cases are implant-based, which has become the most popular method of breast reconstruction following mastectomy [5–7].

Post-mastectomy radiation therapy (PMRT) is often delivered to patients who undergo breast reconstruction using temporary tissue expanders (TEs). Most traditional TEs contain an injection port, which commonly consists of a metal needle guide and a central magnet

that aids in locating the injection site. However, since dose distribution is calculated on computed tomography (CT), these high-density materials may lead to altered dosimetry and inaccurate dose distribution during RT planning [8]. Recently, TEs that make use of a radio frequency identification (RFID) port have been developed (Motiva Flora®), which have replaced ferromagnetic materials with copper rings and metal needle guides with plastic. Therefore, it can be assumed that these structural differences will reduce the distortion of CT images and improve the accuracy of the dose calculation algorithms. As such, there is a need to dosimetrically study strategies designed to reduce the effect of metallic ports.

The purpose of this study was to compare the dosimetric effect of traditional metallic ports and RFID ports on post-mastectomy volumetric modulated arc therapy (VMAT) planning for left-sided breast cancer.

## 2. Materials and Methods

### 2.1. Tissue Expander

To evaluate the dosimetric effect of metallic and RFID ports on post-mastectomy VMAT planning, two products were tested: a conventional TE with a magnetic port and a magnet-free TE with an RFID port (Motiva Flora® TE (Establishment Labs®, Alajuela, Costa Rica)). Compared to magnet ports, RFID ports offer conditional magnetic resonance imaging (MRI) compatibility, thereby reducing the frequently encountered artifacts in conventional TEs [9]. The characteristics of each port are summarized in Table 1, and the schematic diagram of the RFID port is shown in Figure 1.

**Table 1.** Characteristics of breast tissue expanders.

| Parameter | Traditional Expander | Motiva Flora® |
|---|---|---|
| Identification of port location | Magnet | RFID coil |
| Material | Neodymium | Copper |
| Density | 7.01 g/cm$^3$ | 8.96 g/cm$^3$ |
| Diameter | 13.3 mm * | Outer: 24.7 mm<br>Inner: 20.3 ± 0.2 mm |
| Height | 4.4 mm * | 2.150 ± 0.1 mm |
| Needle guide | | |
| Material | Stainless steel | Polyetheretherketone |
| Density | 7.5~8 g/cm$^3$ | 1.3 g/cm$^3$ |
| Diameter | 36.5 mm * | Dome: 40.1 mm *,<br>Needle stop: 26.8 mm *<br>Base: 42.5 mm * |
| Height | 10.0 mm * | 12.9 mm * |
| Thickness | 2.1 mm * | 1.5 mm * |

* Average value of five individual measurements. RFID, radio frequency identification device.

### 2.2. Computed Tomography Simulation

CT simulation was performed on an anthropomorphic torso phantom (CT torso phantom CTU-41, Kyoto Kagaku America Inc., Torrance, CA, USA) using a Philips Brilliance CT scanner (Philips Medical Systems, Cleveland, OH, USA) (Figure 2). This was used since phantom materials with radiation absorption approximates to human tissue (heart, aorta, and vena cava: 40 Hounsfield unit (HU); pulmonary vessels: 8 HU; rib cartilage: 90 HU; and liver: 70 HU) and allows scanning under actual clinical settings. To reproduce TE insertion following mastectomy, a male phantom was used with two types of TE, which were equally set to 345 cc and attached on the left chest wall. TEs were adjusted to be in the same position by referring to three-plane CT imaging. Afterwards, 2.5 mm thick axial images were acquired for RT planning. To reduce CT artifacts caused by the metal implants, a commercial metal artifact reduction for orthopedic implants (O-MAR, Philips Medical Systems, Cleveland, OH, USA) was also applied to the CT images.

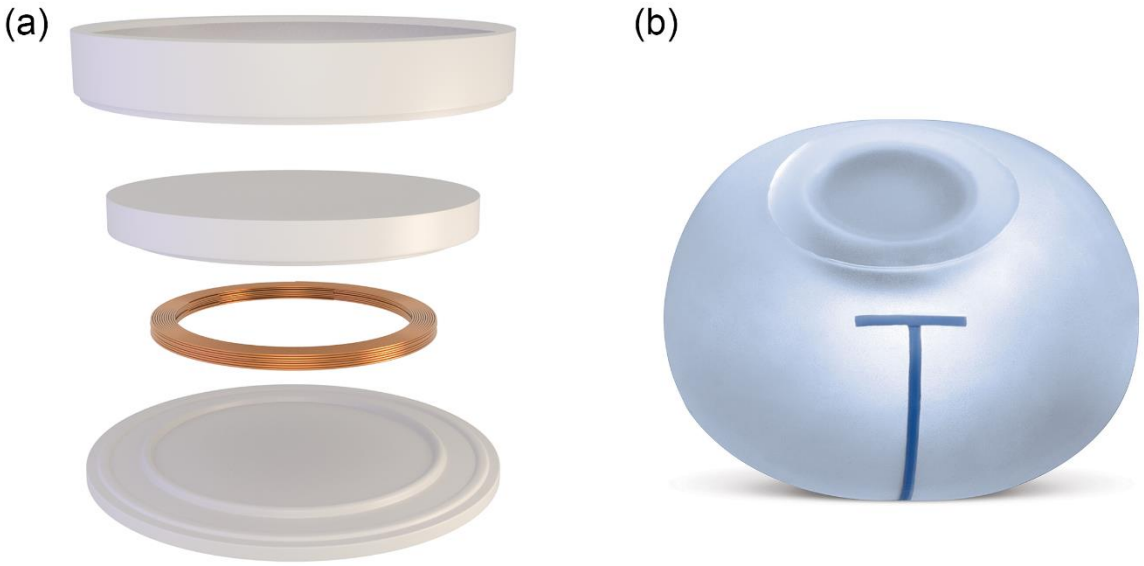


**Figure 1.** The schematic diagram of the radio frequency identification port (**a**) in the Motiva Flora® tissue expander (**b**).


**Figure 2.** Computed tomography simulation. A tissue expander was attached to the left chest wall of the phantom.

### *2.3. Radiation Therapy Planning*

Delineation of the clinical target volume and planning target volume (PTV) was carried out by a physician (M.K.) in accordance to the European Society of Therapeutic Radiology and Oncology-Advisory Committee for Radiation Oncology Practice (ESTRO-ACROP) guidelines [10]. The whole heart was delineated superiorly, starting inferior to the left pulmonary artery and inferiorly blending with the diaphragm [11]. RT planning was performed using the Eclipse™ treatment planning system for Halcyon™ (Varian Medical Systems, Palo Alto, CA, USA). The prescription dose to PTV, which was 50 Gy in 25 fractions, was given at the isodose line, encompassing at least 95% of the PTV while limiting maximum doses to less than 107%. Furthermore, the heart, ipsilateral lung, contralateral lung, whole lung, and contralateral breast were delineated as organs at risk (OAR).

Dose constraints were prescribed based on institutional guidelines (heart: $V_{30Gy}$ (volume receives 30 Gy) < 5%, $D_{mean}$ (mean dose) < 5 Gy; contralateral breast: $D_{mean}$ < 3 Gy; ipsilateral lung: $D_{mean}$ < 7 Gy; contralateral lung: $D_{mean}$ < 3 Gy; whole lung $V_{20Gy}$ < 10%, $D_{mean}$ < 5 Gy). A 5 mm thick bolus was created and placed on the surface of the TEs for each CT image using the Eclipse$^{TM}$ treatment planning system.

VMAT planning using two partial arcs (collimator angle: 130–285) with a single isocenter was generated using a 6 MV flattening-filter-free photon beam with a maximum dose rate of 800 MU/min. The VMAT plan was further optimized using the Eclipse photon optimization algorithm, and the Acuros XB algorithm (version 16.1) was used for dose calculation.

### *2.4. Computed Tomography Image Analysis*

To compare CT artifacts, five points of interest were selected by the physician: point A = central chest wall, point B = medial chest wall, point C = lateral chest wall, point D = axilla, and point E = left anterior descending artery (LAD). The main target volume of PMRT is the chest wall (Points A, B, and C). The axillary lymph nodes are often the location most affected by breast cancer and are represented by point D as axilla level I. Radiation dose to LAD is possible risk factor for cardiac complication. Although it was not possible to contour the LAD exactly, it was contoured to represent the position in relation to human anatomy. The HUs of each point were measured on 10 consecutive slices (Figure 3), and the average HU between the RFID and metallic ports were compared. Using a 10 mm diameter cursor on each slice, the corresponding reference CT numbers within the points were determined on the phantom without the tissue expanders to prevent metal artifacts on the same image set. The HUs were measured on the same CT images as described in Section 2.3 without bolus insertion.

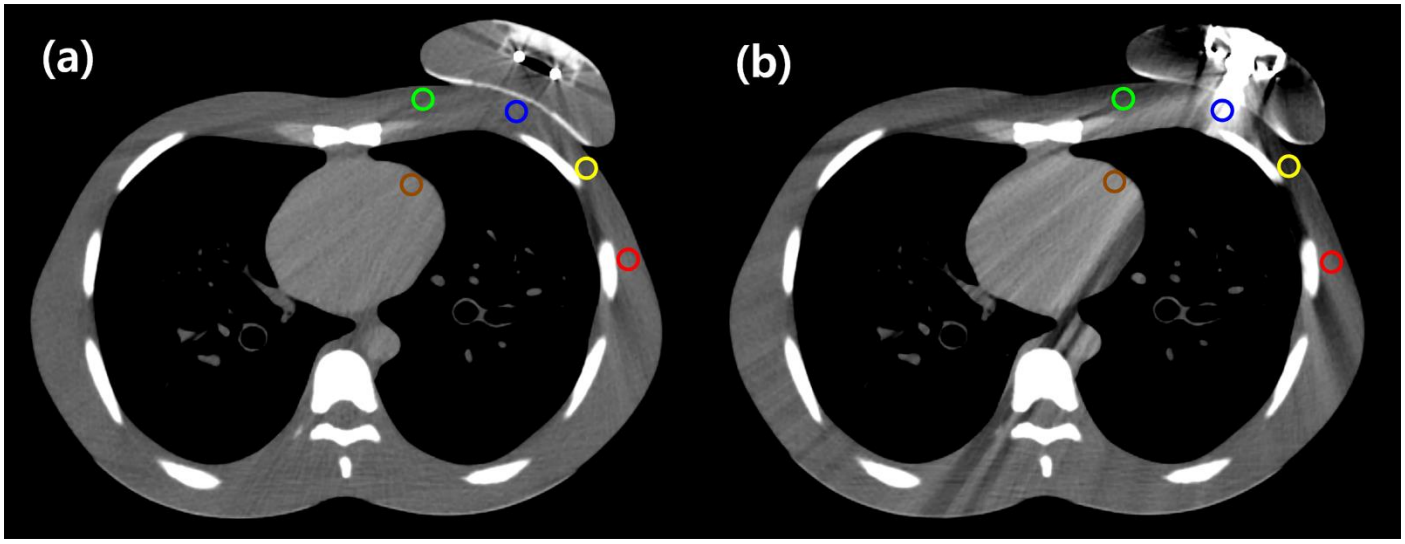


**Figure 3.** An example of the CT image (**a**) RFID port, (**b**) metallic port analysis using the five reference points; point A—central chest wall (blue), point B—medial chest wall (green), point C—lateral chest wall (yellow), point D—axilla (red), point E—left anterior descending artery (brown).

### *2.5. Assessment of Plan Quality*

As proposed by the Radiation Therapy Oncology Group (RTOG), the homogeneity index (HI), conformity index (CI), and quality of coverage (QOC) were used to evaluate dose distribution, which represents the conformance between the prescription dose and PTV, the degree of uniformity inside the PTV, and the dose fall-off outside the PTV [12]. HI was calculated with the formula: HI = $I_{max}$/RI, where Imax is the maximum isodose in the target, and RI is the reference isodose. CI was calculated with the formula: CI = $V_{RI}$/TV, where $V_{RI}$ is the reference isodose volume, and TV is the target volume. Lastly, QOC was

calculated with the formula: QOC = $I_{min}$/RI, where $I_{min}$ is the minimum isodose in the target. Parameters for OAR were also compared.

### 2.6. Statistical Analysis

To compare the parameters between the RFID and metallic ports, the percentage difference was calculated, which was defined as the absolute value of the change in value divided by the average of the two values as seen in Equation (1). The HU differences were calculated using Equation (2).

$$\% \text{ difference} = |\text{Value 1} - \text{Value 2}| \div ([\text{Value 1} + \text{Value 2}]/2) \times 100 \quad (1)$$

$$\text{HU difference} = \text{HU in CT without tissue expander} - \text{HU in CT with tissue expander.} \quad (2)$$

The quality of CT images was compared using the Wilcoxon signed-rank tests. For all statistical analyses, the IBM SPSS Statistics for Windows, version 25.0 (IBM Corp., Armonk, NY, USA) was used, and results were considered statistically significant at $p < 0.05$.

## 3. Results

Table 2 summarizes the results of CT image analysis. As compared with metallic ports, RFID ports tremendously decreased the distortion on CT images, with the exception of point D (axilla). In point E (LAD), the average HU difference for the reference values of the RFID and metallic ports were −2.86 ($p = 0.059$) and −15.16 ($p = 0.005$), respectively. In addition, both ports showed statistically significant average HU differences for the reference values in points A, B, and C on the chest wall.

**Table 2.** Comparison of Hounsfield units.

| Points of the Reference ROIs | RFID Port | | | Metallic Port | | |
|---|---|---|---|---|---|---|
| | Averaged HU | Averaged HU Difference | *p*-Value | Averaged HU | Averaged HU Difference | *p*-Value |
| A (central chest wall) | −2.73 | −18.33 | 0.043 | 118.57 | −139.63 | 0.007 |
| B (medial chest wall) | −19.36 | 8.17 | 0.028 | −34.62 | 23.43 | 0.017 |
| C (lateral chest wall) | −37.36 | 14.93 | 0.028 | −74.37 | 51.94 | 0.005 |
| D (axilla) | −0.92 | −15.14 | 0.005 | −12.32 | −3.74 | 0.169 |
| E (left anterior descending artery) | 32.41 | −2.86 | 0.059 | 44.71 | −15.16 | 0.005 |

ROI, region of interest; RFID, radio frequency identification device; HU, Hounsfield unit.

Table 3 summarizes the results of the dosimetric parameters for PTVs and OARs between the RFID and metallic ports. Dose distributions for the RFID and metallic ports in the axial view are shown in Figure 4. The volumes of $PTV_{RFID}$ and $PTV_{magnet}$ were 921.65 $cm^3$ and 951.9 $cm^3$, respectively. The optimization algorithm was balanced for the PTV coverage, and planned PTV coverage for both the metallic and RFID ports was acceptable. The percentage differences between HI, CI, QOC, and V95 of the PTV for both ports narrowly ranged from 0 to 2.19. However, $V_{107}$ of the PTV was 71.70% for RFID ports and 80.80% for metallic ports, indicating a percentage difference of 11.93. The $V_{5Gy}$, $V_{10Gy}$, $V_{15Gy}$, $V_{20Gy}$, $V_{30Gy}$, and $D_{mean}$ values of the heart in the RFID ports were lower than those in the metallic ports. Specifically, the percentage differences between the RFID and metallic ports was 25.97 (22.91% vs. 29.75%) for $V_{5Gy}$, 54.66 (6.54% vs. 11.46%) for $V_{10Gy}$, 56.84 (2.77% vs. 4.97%) for V15Gy, 65.70 (1.39% vs. 2.75%) for $V_{20Gy}$, 98.90 (0.23% vs. 0.68%) for $V_{30Gy}$, and 18.66 (4.08 Gy vs. 4.92 Gy) for $D_{mean}$. Similarly, the $V_{5Gy}$, $V_{15Gy}$, $V_{20Gy}$, $V_{30Gy}$, and $D_{mean}$ values of the ipsilateral lung in the RFID port were also lower than those in the metallic port. For the ipsilateral lung, the percentage differences between the RFID and metallic ports was 7.41 (36.08% vs. 38.86%) for $V_{5Gy}$, 13.63 (12.85% vs. 14.73%) for $V_{15Gy}$, 14.47 (7.50% vs. 8.67%) for $V_{20Gy}$, 23.16 (1.87% vs. 2.36%) for $V_{30Gy}$, and 7.62 (6.94 Gy vs. 7.62 Gy) for $D_{mean}$. Our results showed that higher $V_{DGy}$ values were

associated with greater percentage differences in the heart and ipsilateral lung. Dose-volume histogram for PTV and OARs in RT plans of both RFID port and metallic port are shown in Figure 5.

**Table 3.** Assessment of plan quality.

| Parameter | RFID Port | Metallic Port | Percentage Difference |
|---|---|---|---|
| PTV | | | |
| HI | 1.31 | 1.32 | 0.76 |
| CI | 0.95 | 0.95 | 0 |
| QOC | 0.92 | 0.90 | 2.19 |
| $V_{95}$, % | 98.40 | 98.10 | 0.30 |
| $V_{107}$, % | 71.70 | 80.80 | 11.93 |
| Heart | | | |
| $V_{5Gy}$, % | 22.91 | 29.75 | 25.97 |
| $V_{10Gy}$, % | 6.54 | 11.46 | 54.66 |
| $V_{15Gy}$, % | 2.77 | 4.97 | 56.84 |
| $V_{20Gy}$, % | 1.39 | 2.75 | 65.70 |
| $V_{30Gy}$, % | 0.23 | 0.68 | 98.90 |
| $D_{mean}$, Gy | 4.08 | 4.92 | 18.66 |
| Ipsilateral lung | | | |
| $V_{5Gy}$, % | 36.08 | 38.86 | 7.41 |
| $V_{15Gy}$, % | 12.85 | 14.73 | 13.63 |
| $V_{20Gy}$, % | 7.50 | 8.67 | 14.47 |
| $V_{30Gy}$, % | 1.87 | 2.36 | 23.16 |
| $D_{mean}$, Gy | 6.43 | 6.94 | 7.62 |
| Contralateral lung | | | |
| $D_{mean}$, Gy | 2.44 | 2.51 | 2.82 |
| Whole lung | | | |
| $V_{20Gy}$, % | 3.69 | 4.25 | 14.10 |
| $D_{mean}$, Gy | 4.40 | 4.68 | 6.16 |
| Contralateral breast | | | |
| $D_{mean}$, Gy | 2.58 | 2.68 | 3.80 |

RFID, radio frequency identification device; PTV, planning target volume; HI, homogeneity index; CI, conformity index; QOC, quality of coverage; $V_D$, percentage volume receiving D% of the prescribed dose; $V_{DGy}$, percentage volume of a given structure receiving a radiation dose of D Gy; $D_{mean}$, mean dose.

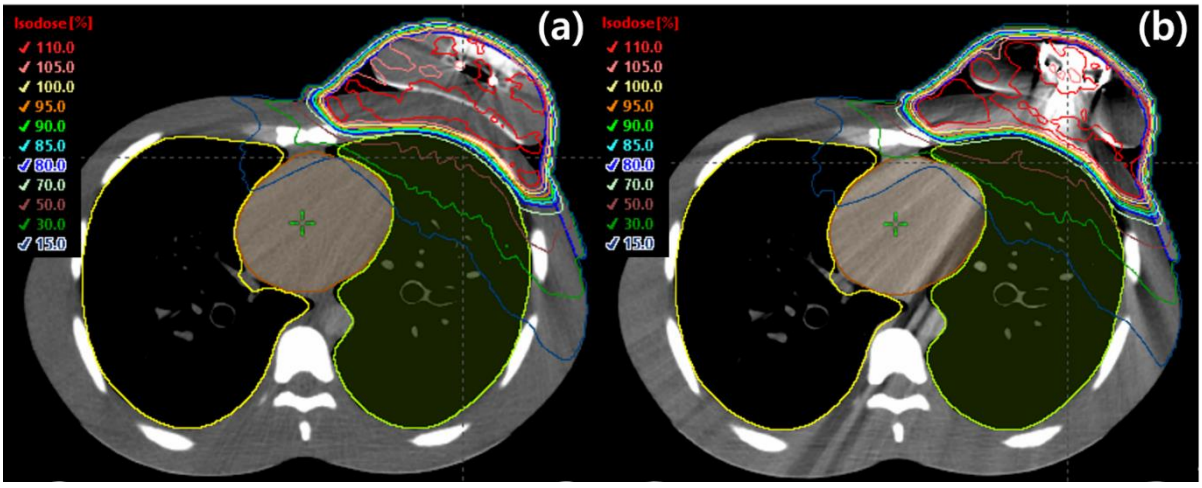


**Figure 4.** The dose distributions for the radio frequency identification ports and metallic ports in axial view. The isodose lines correspond to 110% (red), 105% (pink), 100% (yellow), 95% (orange), 90% (green), 85% (cyan), 80% (blue), 70% (light green), 50% (brown), 30% (dark green), and 15% isodose (dark blue). (**a**) RFID port; (**b**) metallic port.

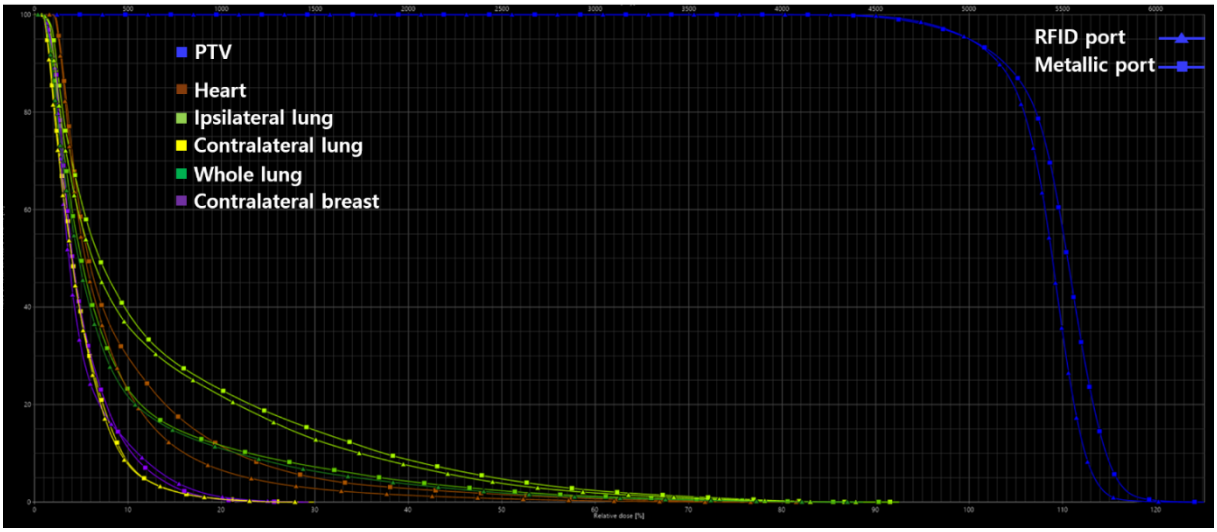


**Figure 5.** Dose-volume histogram for planning target volumes and organs at risk in radiation therapy plans of both radio frequency identification port and metallic port.

## 4. Discussion

Our study compared two types of tissue expanders: those with traditional metallic injection ports and those with RFID ports. We focused on how the dose of RT affected the heart in left-sided breast cancer. We also analyzed how different types of injection ports influenced RT planning and how the dosimetry affected the surrounding normal tissues. In comparison to the metallic ports, the RFID ports showed superior results in terms of RT doses to the heart and lungs as well as in the dosimetric factors related to the target volume.

Currently, most RT planning systems have been developed for CT. However, in the presence of metal implants within or around the target volume, metal artifacts may affect the accuracy required for dose calculation. In fact, many authors have reported on the effects of metallic ports on PMRT. Damast et al. [13], for one, reported their preference of using a permanent implant over TE due to the potential dosimetric effects. Their investigation of single-beam film dosimetry showed that the Magna-Site may attenuate a standard 6 MV photon beam by as much as 22% and a 15 MV beam by 16%. Considering the difference in beam attenuation despite the minimal volume of tissue affected, they recommended the use of a 15 MV photo beam rather than a 6 MV photon beam. Asena et al. [14] also reported reductions of approximately 20% in the photon tangent treatment and 56% in electron boost fields immediately downstream of the implants with magnetic disks.

When treating patients with left-sided breast cancer, measures should be taken to reduce the dose to the heart, as this may increase the risk of heart diseases [15–19]. In addition to this, the present study analyzed the RT doses to the surrounding critical organs. On analysis, RFID ports showed superior results for the doses to the heart and lungs, supporting the notion to keep radiation dose to the heart as low as reasonably achievable. Although metal artifacts vary depending on the size and composition of the metallic port inside the TE, RIFD ports make use of copper rings instead of a solid magnet, thereby reducing the metal volume. Moreover, the RFID ports in this study uses a plastic material, polyetheretherketone (PEEK), as the needle guide, which differs from the stainless steel in conventional TEs. As PEEK has a relatively lower HU than other metals, this potentially reduces the artifacts on CT imaging [20].

Despite these findings, one limitation of the study is that a phantom was used for analysis, which does not accurately reflect the varying chest contours and distance between the heart and target volume in actual practice. Therefore, the comparison of RFID and metallic ports should be further applied and analyzed in different clinical situations. Another limitation was that the metal artifacts were not completely eliminated despite the use of O-MAR.

## 5. Conclusions

The RFID ports (Motiva Flora®) showed superior dosimetric results for doses to the heart and lungs, as compared to traditional metallic ports. Given that PMRT are usually for patients with more advanced breast cancer, minimizing damage to surrounding healthy tissues is more critical. It is expected that risk of side effects may be reduced by decreasing the radiation dose to the heart and lungs by applying an RFID port. However, further studies are needed to assess how RFID ports may affect different types of radiation techniques and clinical outcomes.

**Author Contributions:** Conceptualization, M.K. and N.K.L.; methodology, M.K.; software, J.H.; validation, N.-H.H., M.K. and J.H.; formal analysis, M.K.; investigation, N.-H.H. and J.H.; resources, N.-H.H. and J.H.; data curation, N.-H.H. and M.K.; writing—original draft preparation, N.-H.H.; writing—review and editing, M.K. and N.K.L.; visualization, M.K. and N.K.L.; supervision, N.K.L. and S.L.; project administration, M.K. All authors have read and agreed to the published version of the manuscript.

**Funding:** This work was supported by the Korea University Grant.

**Institutional Review Board Statement:** Not applicable.

**Informed Consent Statement:** Not applicable.

**Data Availability Statement:** The data presented in this study are available in article.

**Conflicts of Interest:** The authors declare no conflict of interest.

## References

1. Mayorov, K.; Ali, E. Magnitude and dosimetric impact of inter-fractional positional variations of the metal port of tissue expanders in postmastectomy patients treated with radiation. *Phys. Imaging Radiat. Oncol.* **2020**, *16*, 37–42. [CrossRef] [PubMed]
2. Cemal, Y.; Albornoz, C.R.; Disa, J.J.; McCarthy, C.M.; Mehrara, B.J.; Pusic, A.L.; Cordeiro, P.G.; Matros, E. A paradigm shift in U.S. breast reconstruction: Part 2. The influence of changing mastectomy patterns on reconstructive rate and method. *Plast. Reconstr. Surg.* **2013**, *131*, 320e–326e. [CrossRef] [PubMed]
3. Radovan, C. Breast reconstruction after mastectomy using the temporary expander. *Plast. Reconstr. Surg.* **1982**, *69*, 195–208. [CrossRef] [PubMed]
4. Bellini, E.; Pesce, M.; Santi, P.; Raposio, E. Two-stage tissue-expander breast reconstruction: A focus on the surgical technique. *BioMed Res. Int.* **2017**, *2017*, 1791546. [CrossRef] [PubMed]
5. Albornoz, C.R.; Bach, P.B.; Mehrara, B.J.; Disa, J.J.; Pusic, A.L.; McCarthy, C.M.; Cordeiro, P.G.; Matros, E. A paradigm shift in U.S. Breast reconstruction: Increasing implant rates. *Plast. Reconstr. Surg.* **2013**, *131*, 15–23. [CrossRef] [PubMed]
6. Farhangkhoee, H.; Matros, E.; Disa, J. Trends and concepts in post-mastectomy breast reconstruction. *J. Surg. Oncol.* **2016**, *113*, 891–894. [CrossRef] [PubMed]
7. Yang, G.; Chang, J.S.; Shin, K.H.; Kim, J.H.; Park, W.; Kim, H.; Kim, K.; Lee, I.J.; Yoon, W.S.; Cha, J.; et al. Post-mastectomy radiation therapy in breast reconstruction: A patterns of care study of the Korean Radiation Oncology Group. *Radiat. Oncol. J.* **2020**, *38*, 236–243. [CrossRef] [PubMed]
8. Papanikolaou, N.; Battista, J.J.; Boyer, A.; Kappas, C. *Tissue Inhomogeneity Corrections for Megavoltage Photon Beams*; AAPM Report No. 85; Task Group No. 85; Task Group No. 65; Medical Physics Publishing: Madison, WI, USA, 2004.
9. Bayasgalan, M.; Munhoz, A.M.; Shellock, F.G. Breast tissue expander with radiofrequency identification port: Assessment of MRI issues. *AJR Am. J. Roentgenol.* **2020**, *215*, 159–164. [CrossRef] [PubMed]
10. Kaidar-Person, O.; Vrou Offersen, B.; Hol, S.; Arenas, M.; Aristei, C.; Bourgier, C.; Cardoso, M.J.; Chua, B.; Coles, C.E.; Engberg Damsgaard, T.; et al. ESTRO ACROP consensus guideline for target volume delineation in the setting of postmastectomy radiation therapy after implant-based immediate reconstruction for early stage breast cancer. *Radiother. Oncol.* **2019**, *137*, 159–166. [CrossRef] [PubMed]
11. Feng, M.; Moran, J.M.; Koelling, T.; Chughtai, A.; Chan, J.L.; Freedman, L.; Hayman, J.A.; Jagsi, R.; Jolly, S.; Larouere, J.; et al. Development and validation of a heart atlas to study cardiac exposure to radiation following treatment for breast cancer. *Int. J. Radiat. Oncol. Biol. Phys.* **2011**, *79*, 10–18. [CrossRef] [PubMed]
12. Shaw, E.; Kline, R.; Gillin, M.; Souhami, L.; Hirschfeld, A.; Dinapoli, R.; Martin, L. Radiation Therapy Oncology Group: Radiosurgery quality assurance guidelines. *Int. J. Radiat. Oncol. Biol. Phys.* **1993**, *27*, 1231–1239. [CrossRef]
13. Damast, S.; Beal, K.; Ballangrud, A.; Losasso, T.J.; Cordeiro, P.G.; Disa, J.J.; Hong, L.; McCormick, B.L. Do metallic ports in tissue expanders affect postmastectomy radiation delivery? *Int. J. Radiat. Oncol. Biol. Phys.* **2006**, *66*, 305–310. [CrossRef] [PubMed]
14. Asena, A.; Kairn, T.; Crowe, S.B.; Trapp, J.V. Establishing the impact of temporary tissue expanders on electron and photon beam dose distributions. *Phys. Med.* **2015**, *31*, 281–285. [CrossRef] [PubMed]

15. Darby, S.C.; Ewertz, M.; McGale, P.; Bennet, A.M.; Blom-Goldman, U.; Brønnum, D.; Correa, C.; Cutter, D.; Gagliardi, G.; Gigante, B.; et al. Risk of Ischemic Heart Disease in Women after Radiotherapy for Breast Cancer. *N. Engl. J. Med.* **2013**, *368*, 987–998. [CrossRef] [PubMed]
16. Darby, S.C.; McGale, P.; Taylor, C.W.; Peto, R. Long-term mortality from heart disease and lung cancer after radiotherapy for early breast cancer: Prospective cohort study of about 300,000 women in US SEER cancer registries. *Lancet Oncol.* **2005**, *6*, 557–565. [CrossRef]
17. Henson, K.E.; McGale, P.; Taylor, C.; Darby, S.C. Radiation-related mortality from heart disease and lung cancer more than 20 years after radiotherapy for breast cancer. *Br. J. Cancer* **2013**, *108*, 179–182. [CrossRef] [PubMed]
18. Onal, C.; Efe, E.; Guler, O.C.; Yildirim, B.A. Dosimetric comparison of sequential versus simultaneous-integrated boost in early-stage breast cancer patients treated with breast-conserving surgery. *In Vivo* **2019**, *33*, 2181–2189. [CrossRef] [PubMed]
19. Ju, E.; Heo, E.J.; Park, C.G.; Kim, M.; Kim, K.H.; Shim, J.B.; Park, Y.J.; Lee, N.K.; Kim, C.Y.; Lee, S. Dosimetric comparison of VitalBeam® and Halcyon™ 2.0 for hypofractionated VMAT with simultaneous integrated boost treatment of early-stage left-sided breast cancer. *J. Appl. Clin. Med. Phys.* **2021**, *22*, 232–238. [CrossRef] [PubMed]
20. Lommen, J.; Schorn, L.; Sproll, C.; Haussmann, J.; Kübler, N.R.; Budach, W. Reduction of CT artifacts using polyetheretherketone (PEEK), polyetherketoneketone (PEKK), polyphenylsulfone (PPSU), and polyethylene (PE) reconstruction plates in oral oncology. *J. Oral Maxillofac. Surg.* **2022**. [CrossRef] [PubMed]